Electronic Supplementary Information for:

Synergistic Effect of Processing Additives and Thermal Annealing in Organic Solar Cells: the Morphology of Magic

Xunfan Liao[a], Ruizhi Lv[a], Lie Chen*[a,b] and Yiwang Chen*[a,b]

[a]College of Chemistry, Nanchang University, 999 Xuefu Avenue, Nanchang 330031, China

[b]Jiangxi Provincial Key Laboratory of New Energy Chemistry/Institute of Polymers, Nanchang University, 999 Xuefu Avenue, Nanchang 330031, China

1. Materials

All reactions and manipulations were operated under argon atmosphere and all the starting materials were purchased from commercial suppliers and used without further purification. Chloroform, Ag (99.999%), MoO_3 (99.999%), $PC_{61}BM$ (99.9%), $PC_{71}BM$ (99.9%) and other materials were purchased from Alfa, or Aldrich and without further purification. Indium-tin oxide (ITO) glass was purchased from Delta Technologies Limited, whereas PEDOT:PSS (Baytron PAl4083) was obtained from Bayer Inc. 4,7-Bis(5-bromothiophene-2-yl)-5,6-difluorobenzo[c][1,2,5]thiadiazole were purchased from Derthon. Tetrakis(triphenylphosphine)palladium(0) [Pd(PPh3)4] was obtained from Energy Chemical.

2. Experimental

The ^{1}H NMR spectra were recorded in deuterated solvents on a Bruker ADVANCE 400 NMR Spectrometer. ^{1}H NMR chemical shifts were reported in ppm downfield from tetramethylsilane (TMS) reference using the residual protonated solvent as an internal standard. Thermogravimetric analysis (TGA) was carried out on a PerkinElmer TGA 7 instrument for thermal analysis at a heating rate of 10 °C min^{-1} under nitrogen. Differential scanning calorimetry (DSC, Perkin-Elmer DSC 7 differential scanning calorimeter) was employed to investigate the phase-transition temperatures of the liquid crystalline small molecule with a constant heating–cooling rate of 10 ºC min^{-1}. UV-vis absorption spectra were recorded on a Perkin Elmer Lambda 750 spectrophotometer. Cyclic voltammetry (CV) was performed a Zahner

IM6e electrochemical workstation. X-ray diffraction (XRD) was performed on a Bruker D8 Focus X-ray diffractometer operating at 30 kV and 20 mA with a copper target (λ= 1.54 Å) and at a scanning rate of 1°/min. The grazing incidence X-ray diffraction (GIXRD) profiles were recorded by using a Bruker D8 Discover reflector with an X-ray generation power of 40 kV tube voltage and 40 mA tube current. In order to increase the effective X-ray penetrating depth and minimize the background from the substrate scattering, the angle between the incident beam and the film surface was fixed at 0.2º. Optical microscopy (OM) images were carried on a Nikon E600POL polarizing optical microscope. Atomic force microscopic (AFM) images were carried on a Nanoscope III A (Digital Instruments) scanning probe microscope using the tapping mode. The specimen for AFM measurement was prepared as same as the devices fabrication other than without MoO_3/Ag was vacuum evaporated on the active layer. Transmission electron microscopy (TEM) images were performed on a JEOL-2100F transmission electron microscope and an internal charge-coupled device (CCD) camera. The specimen for TEM measurement was prepared by spin casting the blend solution on ITO/PEDOT:PSS substrate, then floating the film on a water surface, and transferring to TEM grids.

Space-charge-limited-current (SCLC) mobility measurement. The hole-only devices used a diode configuration of ITO/PEDOT:PSS/active layer/MoO_3/Ag by taking current-voltage curve in the range of 0-6 V. The carrier mobilities were measured using the SCLC model, which is described by $J = 9\varepsilon_0\varepsilon_r u V^2/8L^3$, where J is the current density, L is the film thickness of active layer, ε_0 is the permittivity of free space (8.85×10^{-12} F m^{-1}), ε_r is the relative dielectric constant of the transport medium, u is the hole or electron mobility, V is the internal voltage in the device and $V = V_{appl}$-V_r-V_{bi}, where V_{appl} is the applied voltage to the device, V_r is the voltage drop due to contact resistance and series resistance across the electrodes, and V_{bi} is the built-in voltage due to the relative work function difference of the two electrodes.[1-3] The thickness of the BHJ blend for SCLC measurement was about 90 nm. The hole-mobility can be calculated from the slope of the $J^{1/2}$~V curves.

Fabrication and characterization of OSCs: Organic solar cells (OSCs) were fabricated in the configuration of the traditional sandwich structure of ITO/ZnO/active layer/MoO_3/Ag. ITO-coated glass was cleaned by ultrasonic agitation in acetone, detergent, deionized water and isopropanol sequentially followed by Plasma treatment for 2 min. Then the ZnO precursor solution was spin-cast on the ITO glass at 4000 rpm for 1 min and annealed at 205 °C for 1 h in air to yield an approximately 30 nm film thickness. The devices were transferred into a glovebox filled with N_2. The active layer was prepared by spin-casting the solution of the organic compound donor (D) and $PC_{61}BM$ or $PC_{71}BM$ acceptor (A) with different D/A ratios on the top of the ZnO layer. The concentration of the solution was 18 mg mL^{-1} in chloroform (CF) (or with 0.5 v/v% 1-CN). Then the device was annealed at 130 ^oC for different time. Finally, MoO_3 (7 nm)/Ag (90 nm) was vacuum evaporated on the active layer under a shadow mask in a vacuum of ca. 10^{-4} pa. The active layer area of the device is 4 mm^2. The light source was calibrated by using silicon reference cells with an AM 1.5 Global solar simulator with an intensity of 100 mW cm^{-2}. The current–voltage (*J–V*) characteristics were measured with a Keithley 2400 source meter (Abet Solar Simulator Sun 200). All the measurements were performed under an ambient atmosphere at room temperature. The *EQE* was measured under monochromatic illumination (Oriel Cornerstone 260 1/4 monochromator equipped with Oriel 70613NS QTH lamp), and the calibration of the incident light was performed with a monocrystalline silicon diode.

Synthetic procedures.

Synthesis of 4-(5-bromo-4-hexylthiophen-2-yl)-7-(3,5'-dihexyl-[2,2'-bithiophen]-5-yl)-5,6-difluorobenzo[c][1,2,5]thiadiazole (compound 3): A solution of compound 1 (1.2 g, 1.81 mmol) and compound 2 (0.83 g, 1.81 mmol) in dry toluene (20 mL) was degassed thrice with nitrogen followed by the addition of $Pd(PPh_3)_4$ (125.5 mg, 0.11 mmol). After being stirred at 90 °C for 12 h under nitrogen, the reaction mixture was cooled to room temperature and then dissolved in CH_2Cl_2,

washed with water and dried by anhydrous magnesium sulfate. After evaporation of the solvent, the crude product was purified by column chromatography on silica gel using a mixture of dichloromethane and petroleum ether (1:6) as the eluant to afford compound 3 (0.83 g, 61%) as a red solid. ^{1}H NMR (400 MHz, CDCl3) δ (ppm): 7.96 (s, 1H), 7.95 (s, 1H), 7.06 (d, 1H), 6.76 (d, 1H), 2.84 (t, 4H), 2.55 (t, 2H), 1.72 (m, 6H), 1.52-1.34 (m, 12H), 0.91 (t, 9H).

Synthesis of 7,7'-(5,5'-(4,8-bis(5-(2-ethylhexyl)thiophen-2-yl)benzo[1,2-b:4,5-b']dithiophene-2,6-diyl)bis(4-hexylthiophene-5,2-diyl))bis(4-(3,5'-dihexyl-[2,2'-bithiophen]-5-yl)-5,6-difluorobenzo[c][1,2,5]thiadiazole) (TBDT-T6ffBT): A solution of compound 3 (350 mg, 0.47 mmol) and 4 (170 mg, 0.19 mmol) in dry toluene (10 mL) was degassed thrice with nitrogen followed by the addition of $Pd(PPh_3)_4$ (13 mg, 0.011 mmol). After the reaction being stirred at 110 °C for 24 h under a nitrogen atmosphere, the reaction mixture was cooled to room temperature and then dissolved in chloroform, washed with water and dried by anhydrous magnesium sulfate. After the removal of the solvent, the crude product was purified by column chromatography on silica gel using chloroform and petroleum ether (1:2) as the eluant to obtain a metallic purple solid. The crude product was recrystallized using chloroform and petroleum ether three times to afford TBDT-T6ffBT (291 mg, 80%) as a metallic purple solid and was characterized by HTGC (>99%). ^{1}H NMR (400 MHz, CDCl3) δ (ppm): 8.01 (s, 4H), 7.62 (s, 2H), 7.39 (d, 2H), 6.96 (d, 4H), 6.70 (d, 2H), 2.74-2.93 (m, 16H), 1.68 (m, 12H), 1.33–1.44 (m, 40H), 0.91–1.01 (m, 24H).

Synthesis of 7,7'-(5,5'-(4,8-bis((2-ethylhexyl)oxy)benzo[1,2-b:4,5-b']dithiophene-2,6-diyl)bis(4-hexylthiophene-5,2-diyl))bis(4-(3,5'-dihexyl-[2,2'-bithiophen]-5-yl)-5,6-difluorobenzo[c][1,2,5]thiadiazole) (OBDT-T6ffBT): The synthesis and purification processes of OBDT-T6ffBT are similar to those of TBDT-T6ffBT, but monomer 4 was used instead of 5. The obtained OBDT-T6ffBT is also a metallic purple solid with ca. 78% yield. 1H NMR (400 MHz, CDCl3) δ (ppm): 8.06 (s, 4H), 7.44 (s, 2H), 6.99 (d, 2H), 6.71 (d, 2H), 4.18 (d, 4H), 2.75 (t, 12H), 1.34–1.69 (m, 42H), 0.90–1.01 (m, 20H).

3. Supporting Figures and Tables

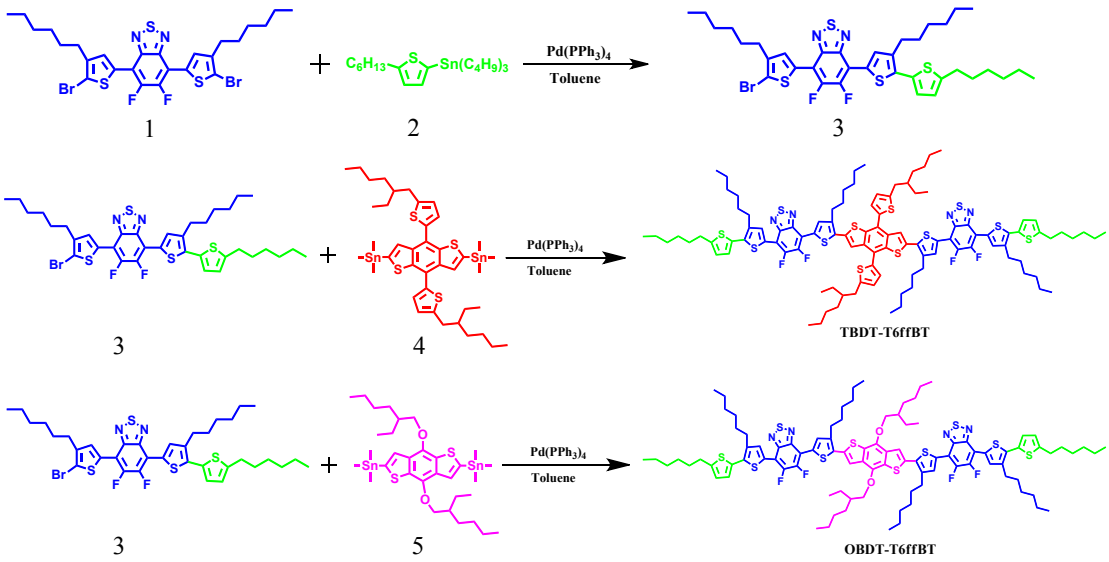

Scheme S1. Synthetic Route of TBDT-T6ffBT and OBDT-T6ffBT

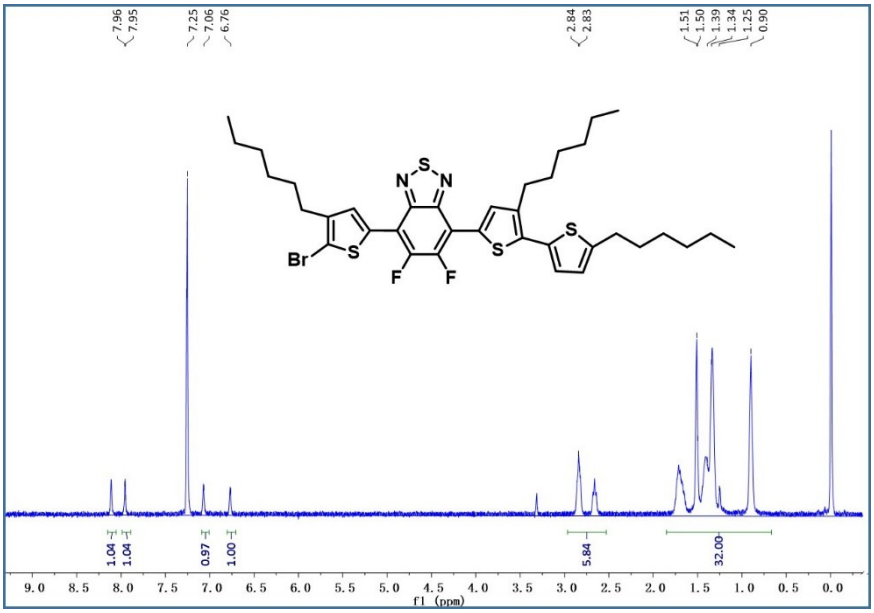

Figure S1. ^{1}H NMR spectra of compound 3 in $CDCl_3$.

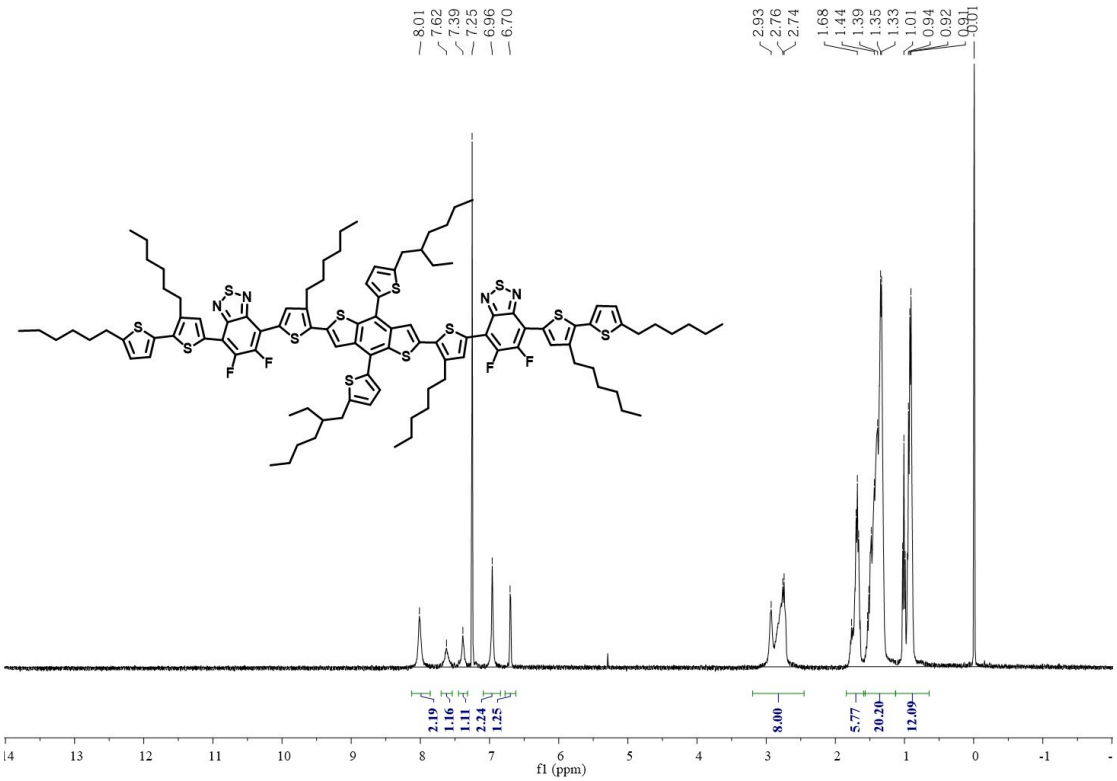

Figure S2. ^{1}H NMR spectra of TBDT-T6ffBT in $CDCl_3$.

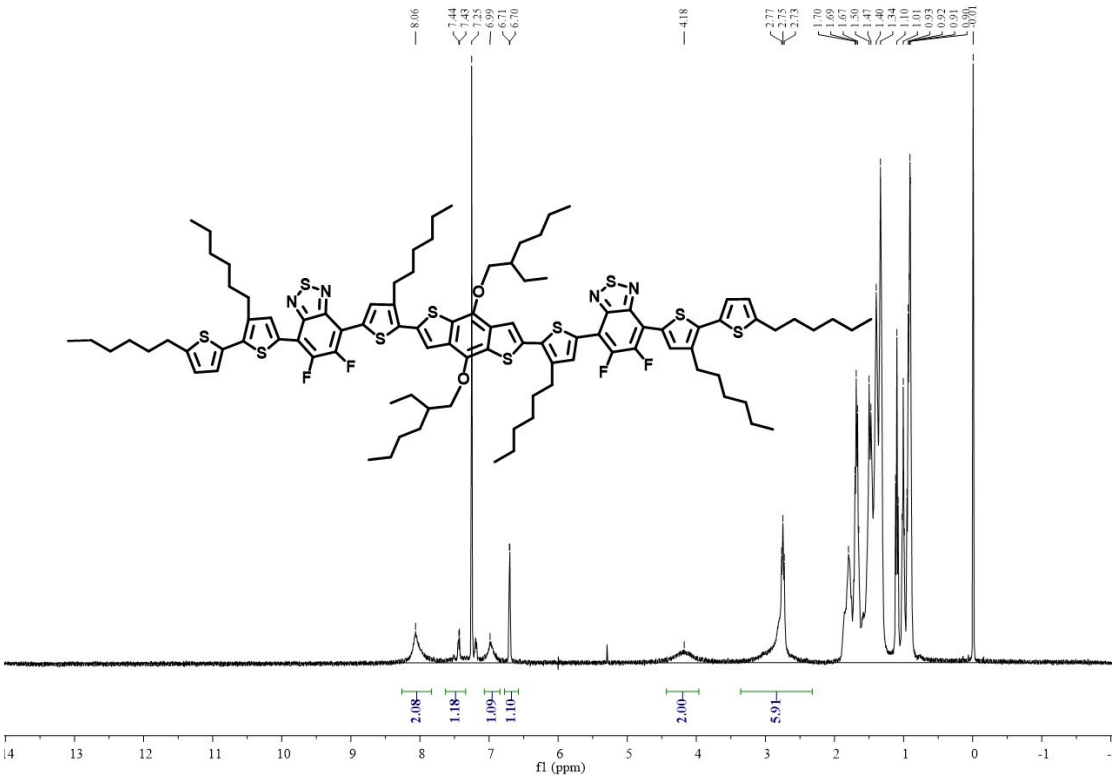

Figure S3. ^{1}H NMR spectra of OBDT-T6ffBT in $CDCl_3$.

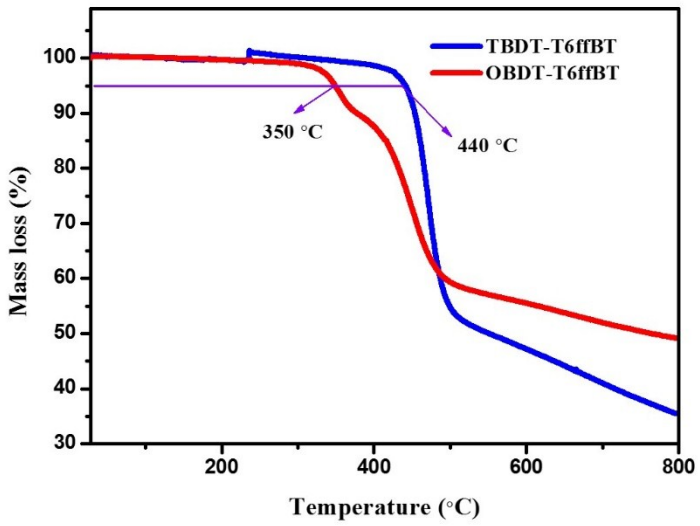

Figure S4. Thermogravimetric analysis (TGA) plot of SMs with a heating rate of 10 ºC min^{-1} under nitrogen atmosphere.

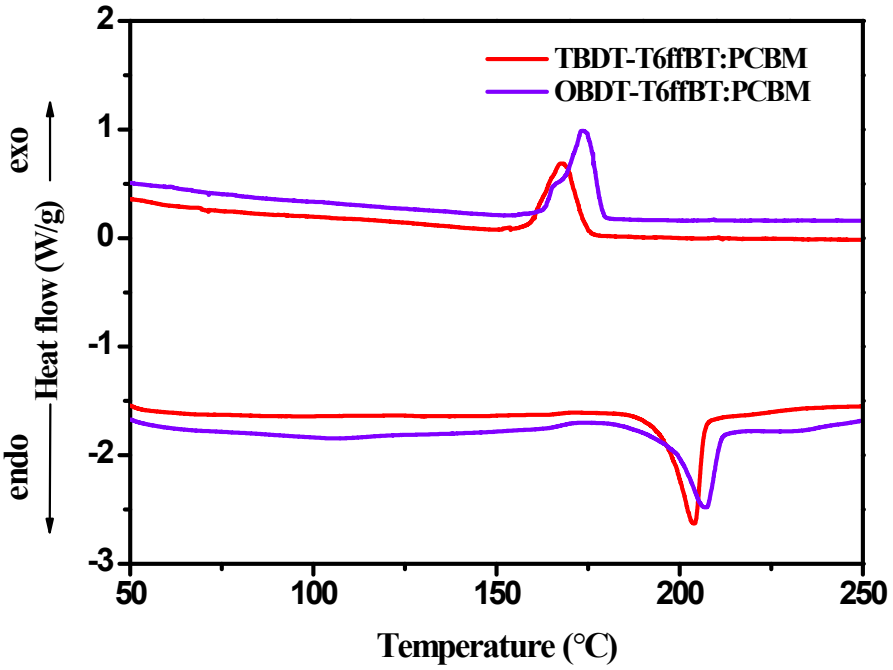

Figure S5. Differential scanning calorimetry (DSC) thermograms of blended films.

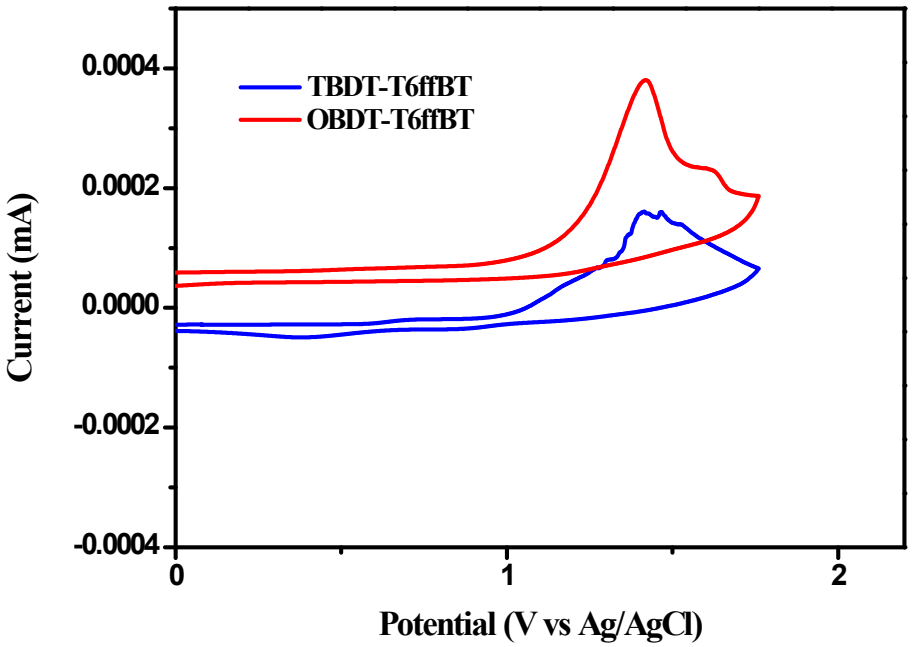

Figure S6. Cyclic voltammogram of the polymers films in a 0.1 mol L^{-1} Bu_4NPF_6/CH_3CN solution at a scan rate of 50 mV s^{-1}.

Table S1. Optical and Electrochemical Properties of Small Molecules (SMs)

SMs	UV-Vis Absorption			E_g^{opt} (eV)[b]	HOMO (eV)[c]	LUMO (eV)[d]
	λ_{max} (solution)[a] (nm)[a]	λ_{max} (film) (nm)	λ_{onset} (film) (nm)			
TBDT-T6ffBT	528	682	716	1.73	-5.29	-3.56
OBDT-T6ffBT	528	584	719	1.72	-5.36	-3.64

[a]Measured in a $CHCl_3$ solution. [b]Determined from the onset of UV-Vis absorption spectra, $Eg^{opt} = 1240/\lambda_{onset}$. [c]Determined from cyclic voltammetry. [d]LUMO = HOMO + Eg, in which the optical energy gap.

Table S2. Summary of Solar Cell Characteristics of TBDT-T6ffBT and OBDT-T6ffBT blend with different ratio of $PC_{61}BM$ or $PC_{71}BM$

Active layer	D/A ratio	V_{oc} (V)	J_{sc} (mA/cm^2)	FF (%)	PCE (%)
TBDT-T6ffBT:$PC_{61}BM$	2:1	0.843	2.94	56.7	1.41
	1:0.8	0.837	5.51	56.2	2.59
	1:2	0.809	4.07	59.3	1.95
TBDT-T6ffBT:$PC_{71}BM$	2:1	0.847	2.91	48.4	1.19
	1:0.8	0.861	4.21	49.5	1.79
	1:2	0.825	3.18	52.4	1.37
OBDT-T6ffBT:PC61BM	2:1	0.769	4.62	48.4	1.72
	1:0.8	0.759	4.84	50.5	1.86
	1:2	0.702	2.92	46.5	0.95
OBDT-T6ffBT:$PC_{71}BM$	1:0.8	0.775	3.69	54.4	1.56

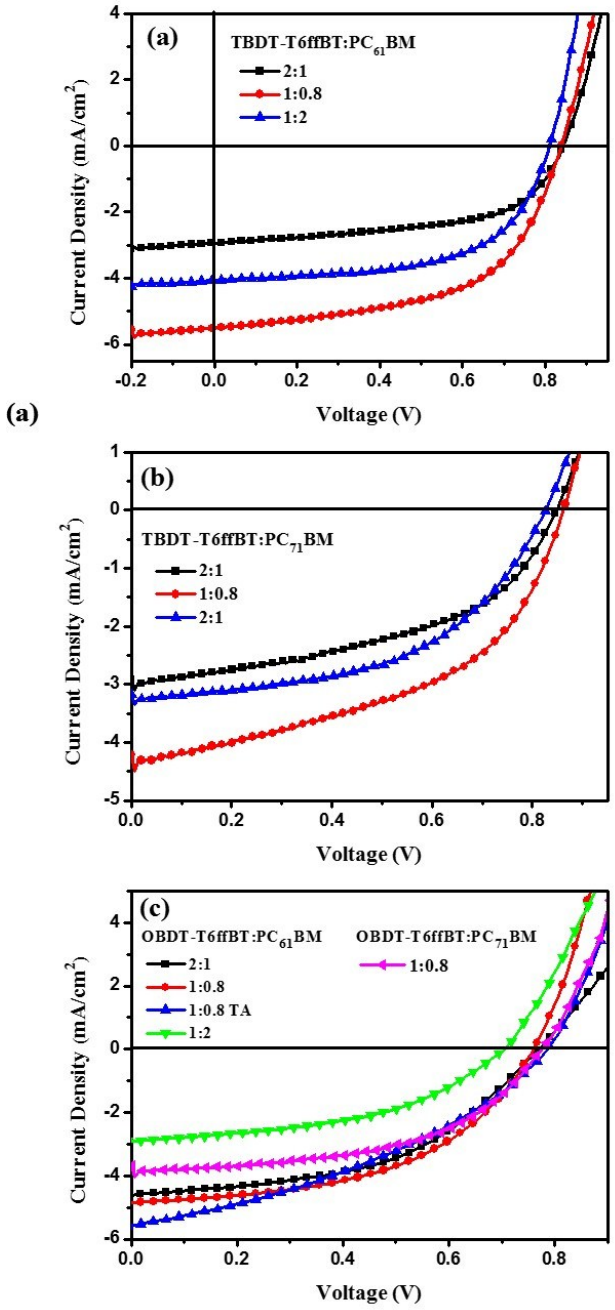

Figure S7. (a) *J-V* curves of BHJ solar cells based on TBDT-T6ffBT:$PC_{61}BM$ and (b) TBDT-T6ffBT:PC71BM with different weight ratios (w/w) under illumination of AM 1.5 G, 100 mW cm^{-2}. (c) *J-V* curves of BHJ solar cells based on OBDT-T6ffBT:$PC_{61}BM$ with different weight ratios and OBDT-T6ffBT:$PC_{71}BM$ with 1:0.8 weight ratio under illumination of AM 1.5 G, 100 mW cm^{-2}.

Table S3. Photovoltaic performance of BHJ solar cells based on OBDT-T6ffBT:$PC_{61}BM$ with weight ratio at 1:0.8 cast from $CHCl_3$ with 1-CN, DIO or DPE under illumination of AM 1.5 G, 100 mW cm^{-2}.

Active layer	Additive	V_{oc} (V)	J_{sc} (mA/cm^2)	FF (%)	PCE (%)
	0	0.759	4.84	50.5	1.9
OBDT-T6ffBT:PC61BM	0.5% 1-CN	0.736	4.55	38.3	1.3
(1:0.8)	0.5% DIO	0.703	4.65	45.0	1.5
	0.5% DPE	0.73	4.97	49.3	1.8

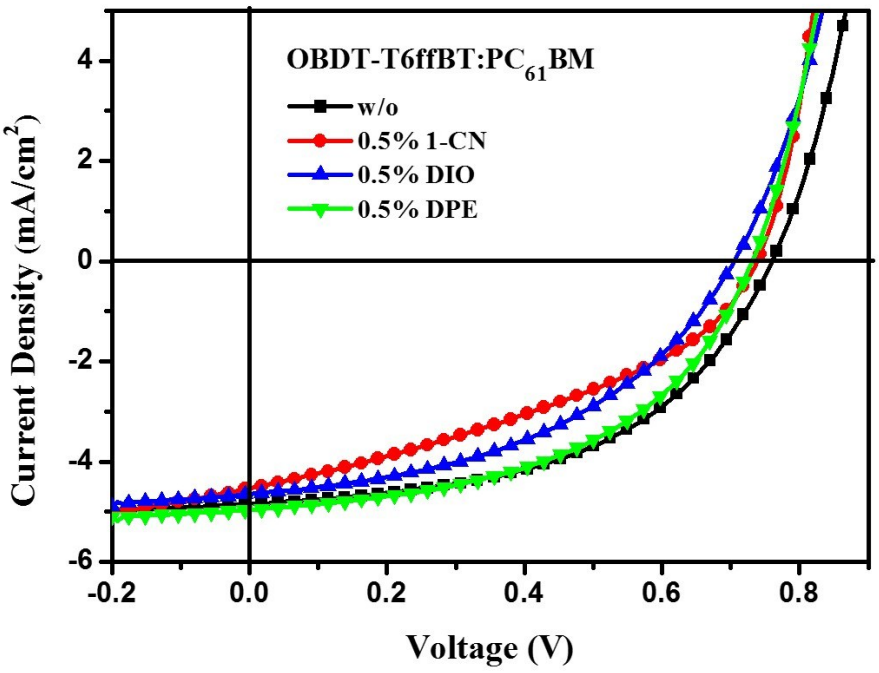

Figure S8. *J-V* curves of BHJ solar cells based on OBDT-T6ffBT:$PC_{61}BM$ with weight ratio at 1:0.8 cast from $CHCl_3$ with 1-CN, DIO or DPE under illumination of AM 1.5 G, 100 mW cm^{-2}.

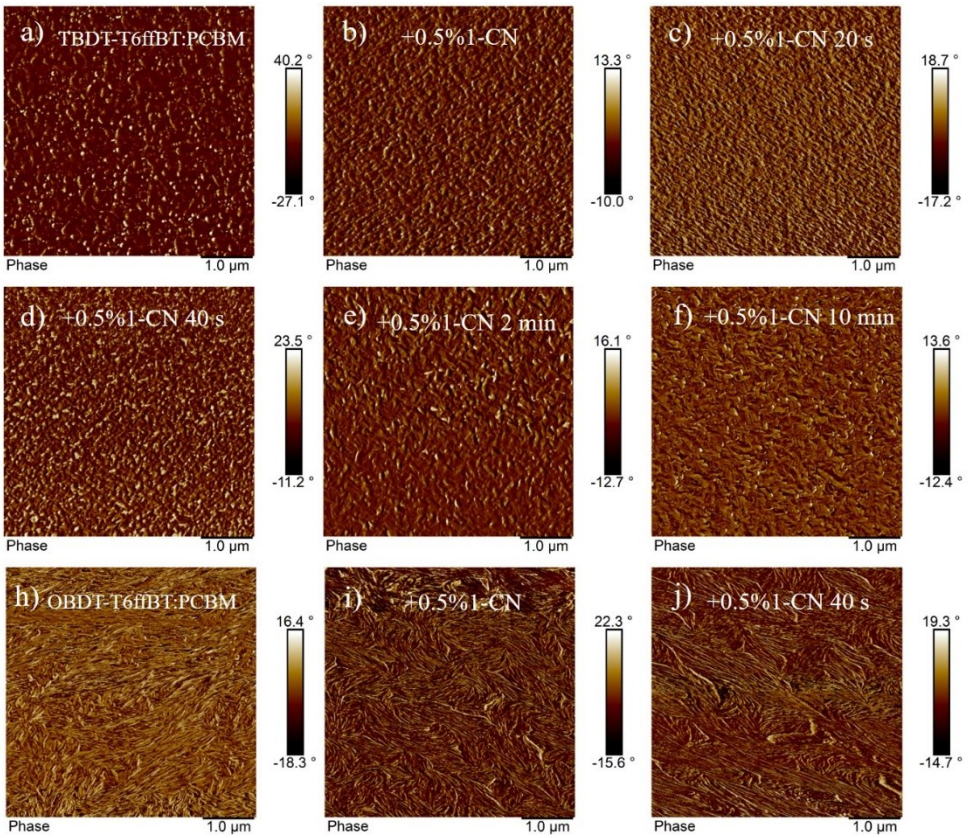

Figure S9. AFM phase images (1 µm × 1 µm) of the active layers: image for TBDT-T6ffBT:PCBM pristine film (a) and (b) with 0.5 v/v% 1-CN additive; image for TBDT-T6ffBT:PCBM with 0.5 v/v% 1-CN additive and further thermal annealing at 130 °C for 20 s (c), 40 s (d), 2 min (e) and (f) 10 min; image for OBDT-T6ffBT:PCBM pristine film (h) and (i) with 0.5 v/v% 1-CN additive; (j) image for OBDT-T6ffBT:PCBM with 0.5 v/v% 1-CN additive and further thermal annealing at 130 °C for 40 s.

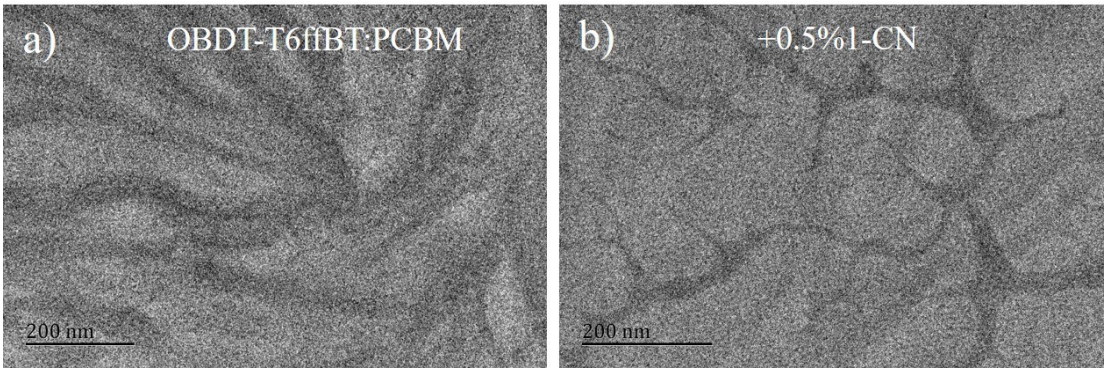

Figure S10. TEM images of the OBDT-T6ffBT:$PC_{61}BM$ blend film with or without 0.5 v/v% 1-CN additive.

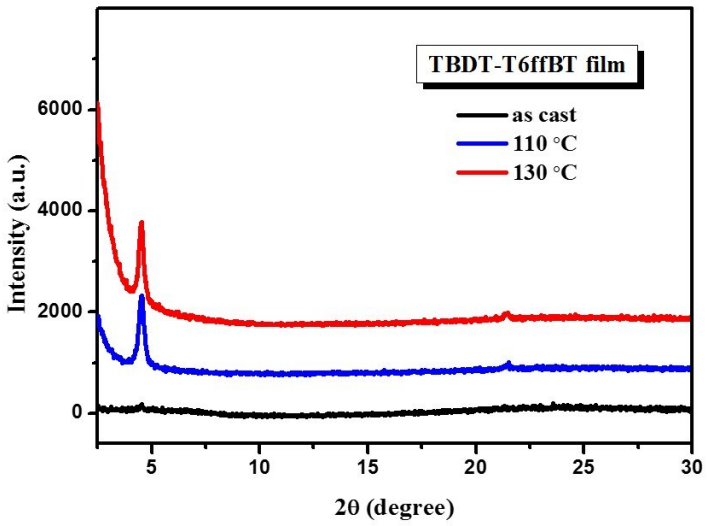

Figure S11. X-ray diffraction patterns of the TBDT-T6ffBT film with or without thermal annealing.

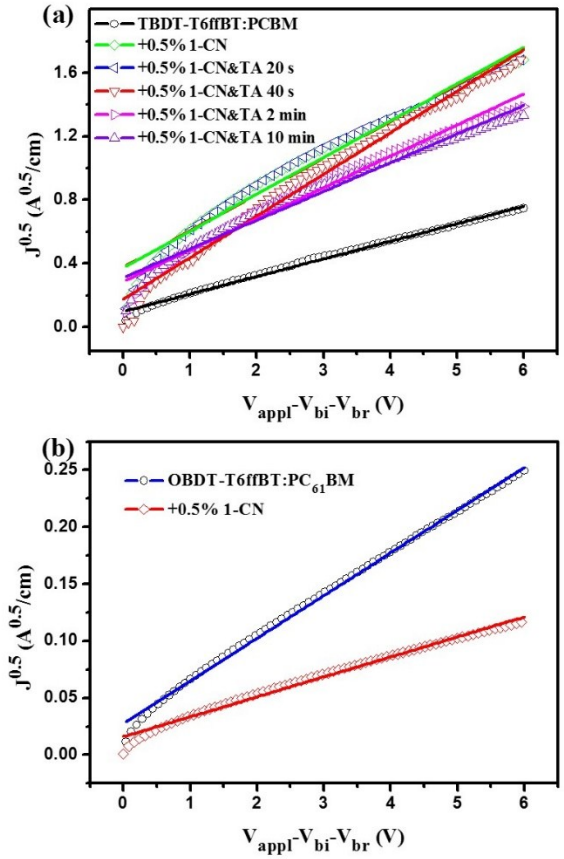

Figure S12. $J^{0.5-V}$ plots of hole-only devices with (a) TBDT-T6ffBT:PC61BM and (b) OBDT-T6ffBT:PC_{61}BM blend film with different treatment.

References:

[1] H. C. Chen, C. W. Lai, I. C. Wu, H. R. Pan, I. Chen, P. Wen, Y. K. Peng, C. L. Liu, C. h. Chen, P. T. Chou, *Adv. Mater.* 2011, 23, 5451.

[2] Y. J. Cheng, C. H. Hsieh, P. J. Li, C. S. Hsu, *Adv. Funct. Mater.* 2011, 21, 1723.

[3] Y. Liu, X. Wan, F. Wang, J. Zhou, G. Long, J. Tian, Y. Chen, *Adv. Mater.* 2011, 23, 5387.